Influence of operating frequency on high-power medium-voltage medium-frequency transformers

Thomas B. Gradinger[1], Ralph M. Burkart, and Marko Mogorovic

Hitachi Energy Switzerland Ltd.
URL: http://www.hitachienergy.com
[1] Segelhofstrasse 1A
5405 Baden-Dättwil, Switzerland
Tel.: +41 (0)79 150 59 69
E-Mail: thomas.gradinger@hitachienergy.com

Keywords

«Solid-state transformer», «medium voltage», «transformer», «design optimization».

Abstract

This paper provides a fundamental insight into the scaling laws of medium-frequency transformers (MFTs). Economic MFTs are a key enabler for solid-state transformers and viable MVDC solutions. An understanding of the influences on the MFT cost structure, and of the limitations to the reduction of size, mass, and cost, is therefore key. Simplified scaling laws are developed that suggest a potential of an increase in switching frequency to improve the MFT performance metrics. They suggest that for fixed MFT geometry, an increase in frequency can lead to lower losses under constrained inductances. The scaling laws also show that a core-size reduction at a given frequency must always be accompanied by increasing core losses. In practical MFT design, size reduction is only observed up to a certain "scaling saturation" frequency. In the studied examples featuring nanocrystalline cores, it is located near 7 kHz. Insight into the scaling behavior is provided by the analysis of the constraint functions used in the MFT optimization. A constrained loss ratio may limit the designs at all frequencies and inhibit core-size reduction. The "scaling saturation" frequency corresponds to a transition between saturation limit and thermal limit of the core, and can be shifted upward by improved core cooling. This enables an attractive compromise between cost savings and loss increase, and shows the importance of sufficient core cooling.

Introduction

Nowadays, the electric distribution grids are facing a proliferation of modern high-power electric applications ranging from several MW to several hundred MW, such as renewables [1], railways [2], e-mobility [3], and data centers [4, 5]. Consequently, the solutions for conversion from high-power MVAC to controlled LVAC or LVDC, and thus the solid-state transformer (SST) concept, are more and more under the focus of the industry [6, 7]. Moreover, the SST is an enabler of the emerging MVDC grids, with the high promise of enabling a significantly more efficient transmission, and an opportunity to increase the capacity of existing MVAC infrastructure by refurbishing and converting it into MVDC [8]. The most popular SST topology is a modular solution consisting of multiple identical cells in a so-called, input-series-output-parallel (ISOP) connection (or vice versa, IPOS, depending on the power-flow direction). The MFT is a key component of each SST cell, providing both input-output voltage matching and galvanic insulation as one of the mandatory features of the SST, as required by standards for interconnection of MV and LV [9].

If we are to analyze the economic viability of an MVDC system based on the total cost of ownership (TCO), this value will depend on the cost of all components, including the SST. Hence, highly efficient and economic solutions for the SST and therefore the MFT, as a significant contributor to the SST cost and losses, are a key. As the cost to be optimized is not CapEx (capital expenditure), but TCO including the cost of losses, optimization of investment cost must be done under constraints of efficiency.

An important choice in the context of cost optimization is that of the operating frequency of the MFT. It is known to have a strong influence on the MFT and can be chosen freely, up to some efficiency limit

of the converters connected to the MFT. With the advent of SiC, the available frequency range has extended even higher, allowing significant freedom of choice that can be used for SST and MFT optimization [10–12]. In their simplest form, the equations governing transformer design suggest a size reduction with frequency [13] according to

$$A_\mathrm{c} A_\mathrm{w} \propto \frac{S}{J f_\mathrm{sw} \hat{B}}, \tag{1}$$

where S and J are apparent power and rms current density, respectively, f_sw is the switching frequency, $\hat{B}$ is the magnetic peak-flux density, and A_c and A_w are the cross-sections of the core and windings, respectively. It has been shown, however, that there are limits to the size reduction. In [10], it was demonstrated that this limit is due to cooling, and that there is an optimum frequency depending on the cooling performance. While the basic findings in this study still appear to be valid, the present study focuses on several important extensions and modifications. Most importantly, these include

- the choice of higher power per MFT, which is important to avoid uneconomically high insulation effort for MV applications;
- the choice of nanocrystalline core material, which covers best the considered range of f_sw of 1 to 15 kHz;
- the consistent consideration of the inductance requirements coming from the converters;
- a detailed and realistic insulation model;
- detailed analysis of the design limits imposed via constraint functions, including temperatures and efficiency, and including the roles of the individual components (core, windings); and
- an analysis of cost, rather than volume and mass, only.

As winding conductor, litz wire is considered in the present study. Next to foil, this is one of the dominant conductor types for medium-frequency windings. The focus on litz wire does not correspond to a loss of generality, because both conductor types are adaptable in sub-conductor size (strand diameter or foil thickness), which is the essential feature in the context of the present study. For the insulation, dry casting, with separately cast LV and HV windings, is assumed.

MFT optimization tool

As a basis for the present study, a MATLAB tool was used for MFT design and optimization. This tool – called *MFT optimization tool* for brevity – is described in [14]. For convenience, a summary of this description is provided here. The core of the tool is a function that evaluates an individual MFT design, based on a technical requirements specification (TRS) and a vector x of *primary variables* that fully define the MFT design. $x = \{x_\mathrm{d}, x_\mathrm{c}\}$ consists of a vector x_d of discrete variables and a vector x_c of continuous variables. Examples of discrete variables are the number of turns N_t of a winding, the strand diameter d_s of litz wire, and the core material. Examples of continuous variables are core-window width Δx_c, core-window height Δz_c, and current density in a winding conductor. x is also called the *design space*, and a particular point within it, i.e., a value of x, is called a *design point*. The MFT optimization tool is versatile and covers different core materials, winding-conductor types, and insulation types. The variables in x and the length of x may change depending on the type of MFT design.

Optimization is done with respect to a cost function u, for which a minimum is sought; and under constraints, expressed by constraint functions K_i. u is a weighted rms of cost (C), mass (m), boxed volume (V_box), and loss ratio, i.e., losses per real power (λ):

$$u \equiv \sqrt{w_c \left(C/C_\mathrm{opt}\right)^2 + w_m \left(m/m_\mathrm{opt}\right)^2 + w_V \left(V_\mathrm{box}/V_\mathrm{box,opt}\right)^2 + w_\lambda \left(\lambda/\lambda_\mathrm{opt}\right)^2}, \tag{2}$$

where the w_z are weighting factors ($z = C, m, V_\mathrm{box}$, or λ), and z_opt is the value of z at the optimum. The constraint functions are used to enforce upper temperature limits of the materials used as well as an upper limit on the loss ratio, and to avoid core saturation. They can also be used to enforce upper and lower limits on magnetizing and leakage inductance. A valid solution has $K_i \leq 0 \; \forall \; i$, while $K_i = 0$ indicates an active constraint. The optimization is based on sweeping x, using gridded interpolants for u and the K_i. The MFT optimization tool is mostly based on simplified physical models that are quick to evaluate, and that describe the electromagnetic and thermal behavior of the MFT and enable the design of the electrical insulation. Typically, analytical expressions [15] are used, equipped with

"engineering coefficients". The insulation model is based on realistic assumptions and includes consideration of the tests required by international standards [16].

Scaling laws

As will be seen, the MFT cost function is strongly influenced by the constraints on the inductances. From the point of view of the converters connected to the MFT, two inductances are key: the magnetizing inductance L_m and the leakage inductance L_σ. Both L_m and L_σ need to assume a certain value, or lie within a certain range, to facilitate converter design. This holds both for LLC resonant converters and for DABs (dual-active bridges). In the following, the constraints for L_m and L_σ are expressed as constraints for L_m and L_m/L_σ. Key geometric parameters of the MFT, that are used in the scaling laws, are identified in Fig. 1. It is noted that the considered MFT has both the primary and secondary winding distributed among both core legs. Each leg is surrounded by a primary-winding portion on the inside, and a secondary-winding portion on the outside. The portions of a winding can be series or parallel connected.

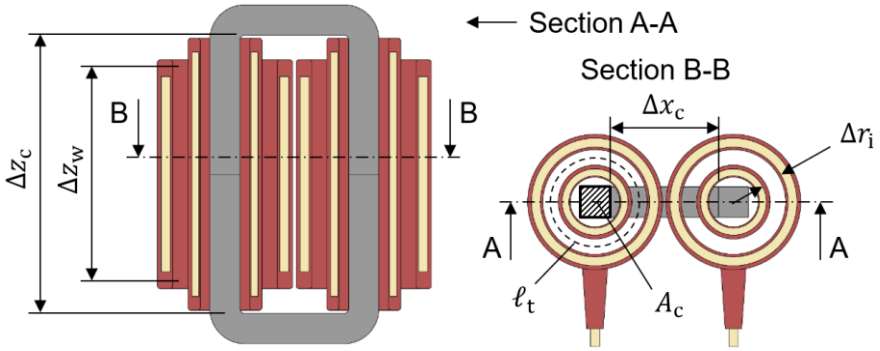

Fig. 1: Key geometric parameters of MFT: mean winding height, Δz_w; core-window height, Δz_c; core-window width, Δx_c; mean turn length, ℓ_t; mean radial distance between windings due to insulation, Δr_i; core cross-section, A_c.

Assuming that the needed mean turn length is mainly influenced by the core cross-section, the leakage inductance scales as follows:

$$L_\sigma \propto \frac{N_\mathrm{t}^2 \ell_\mathrm{t} \Delta r_\mathrm{i}}{\Delta z_\mathrm{w}} \propto \frac{N_\mathrm{t}^2 A_\mathrm{c}^{1/2} \Delta r_\mathrm{i}}{\Delta z_\mathrm{w}}. \tag{3}$$

Δr_i results from the TRS via the insulation requirements, while A_c (via core-leg width) and N_t are part of the design space. Δz_w results from Δz_c after subtracting the insulation distances and can therefore also be considered to be part of the design space.

With R_m denoting the magnetizing reluctance, L_m scales as follows:

$$L_\mathrm{m} \propto \frac{N_\mathrm{t}^2}{R_\mathrm{m}} \propto \frac{N_\mathrm{t}^2 \mu_0 A_\mathrm{c}}{\frac{\ell_\mathrm{c}}{\mu_{\mathrm{r,c}}} + \ell_\mathrm{g}} \propto \frac{N_\mathrm{t}^2 A_\mathrm{c}}{\ell_\mathrm{g}}. \tag{4}$$

Here, ℓ_c and ℓ_g denote the length of the magnetic path in the core and the air-gap width, respectively; and $\mu_{\mathrm{r,c}}$ is the relative permeability of the core. The assumption is made that the reluctance is dominated by the air gap, which is a good design principle that ensures robustness and the possibility for fine-tuning L_m, if needed. After selecting a design point, ℓ_g is adapted to obtain the required L_m.

The saturation constraint for the core is

$$B_\mathrm{sat} \geq \hat{B} = \frac{\hat{\Phi}}{A_\mathrm{c}} \propto \frac{N_\mathrm{t} \hat{I}_\mathrm{m}}{R_\mathrm{m} A_\mathrm{c}} \propto \frac{N_\mathrm{t} \hat{I}_\mathrm{m}}{\ell_\mathrm{g}}, \tag{5}$$

where $\hat{\Phi}$ and $\hat{I}_\mathrm{m}$ are the peaks of the magnetic flux and the magnetizing current, respectively. The amount of magnetizing current is relevant for achieving soft switching in the semiconductors.

For the ratio of inductances, one gets

$$\frac{L_\mathrm{m}}{L_\sigma} \propto \frac{A_\mathrm{c}\Delta z_\mathrm{w}}{\ell_\mathrm{g} A_\mathrm{c}^{1/2}\Delta r_\mathrm{i}} \propto \frac{A_\mathrm{c}^{1/2}\Delta z_\mathrm{w}}{\ell_\mathrm{g}}. \tag{6}$$

From this scaling law, one notes that a high value of L_m/L_σ, which corresponds to good magnetic coupling between primary and secondary, tends to yield a tall MFT with a large core cross-section and a small air gap.

To develop an understanding of the MFT's scaling with the switching frequency f_sw, next, the loss scaling is studied under the assumption that both L_m and L_σ scale with $1/f_\mathrm{sw}$. This assumption is reasonable from the point of view of converter requirements to achieve frequency invariant current shapes with constant rms and corner values. As a starting point, an optimized MFT design at a reference frequency f_sw^* is taken. Then, for $f_\mathrm{sw} > f_\mathrm{sw}^*$, it is assumed that the MFT design does not change, except for N_t. According to (3) and (4), $L_{\{\mathrm{m},\sigma\}} \propto N_\mathrm{t}^2$, such that

$$N_\mathrm{t} \propto f_\mathrm{sw}^{-1/2}. \tag{7}$$

For the core losses P_c, the Steinmetz equation is adopted since it facilitates simple scaling laws. Using (5) and (7),

$$P_\mathrm{c} \propto f_\mathrm{sw}^\alpha \hat{B}^\beta \propto f_\mathrm{sw}^\alpha N_\mathrm{t}^\beta \propto f_\mathrm{sw}^{\alpha-\beta/2}. \tag{8}$$

The Steinmetz parameters α and β depend on the core material. In the present study, the focus is on nanocrystalline material, which is the one that covers best the analyzed frequency range of 1 to 15 kHz. For Vitroperm 500 F, we measured $\alpha = 1.14$ and $\beta = 1.98$, such that

$$P_\mathrm{c} \propto f_\mathrm{sw}^{0.15}. \tag{9}$$

The winding losses P_w depend on the DC resistance R_dc and on the AC-to-DC resistance ratio F_R, which is frequency dependent:

$$P_\mathrm{w} \propto R_\mathrm{dc} F_R(f_\mathrm{sw}). \tag{10}$$

With the overall cross-section of the winding staying the same, the conductor cross-section can grow if there are fewer turns, such that

$$R_\mathrm{dc} \propto \frac{N_\mathrm{t}^2 \ell_\mathrm{t}}{\Delta z_\mathrm{w} F_\mathrm{Cu}} \propto \frac{N_\mathrm{t}^2 A_\mathrm{c}^{1/2}}{\Delta z_\mathrm{w} F_\mathrm{Cu}}, \tag{11}$$

where F_Cu is the copper filling ratio, i.e., the ratio of copper to total litz-wire cross-section. Using (7) and noting that A_c and Δz_w remain constant,

$$R_\mathrm{dc} \propto \frac{1}{f_\mathrm{sw} F_\mathrm{Cu}}. \tag{12}$$

It is assumed that F_R can be kept approximately constant when raising f_sw by reducing the litz-wire's strand diameter d_s such that its ratio to the skin depth δ stays constant. For the frequency range of interest, it suffices to consider d_s in the range of 0.1 to 0.5 mm (AWG, American Wire Gauge, 38 to 24), which is well feasible and commercially available. Since $\delta \propto f_\mathrm{sw}^{-1/2}$, one gets $d_\mathrm{s} \propto f_\mathrm{sw}^{-1/2}$. Reducing d_s generally leads to a reduction of F_Cu, which can be assumed to scale like

$$F_\mathrm{Cu} \propto d_s^\gamma. \tag{13}$$

In the range of d_s of 0.1 to 0.5 mm, $\gamma = 0.4$ is a reasonable assumption. Using (12), one obtains $R_\mathrm{dc} \propto f_\mathrm{sw}^{-0.8}$, such that also

$$P_\mathrm{w} \propto f_\mathrm{sw}^{-0.8}. \tag{14}$$

This suggests significant loss-reduction potential for the windings by increasing the frequency. A potential limiting factor of the reduction of the total MFT losses is the growth of P_c according to (9). However, since the exponent of 0.15 of P_c is small, the growth of P_c should not dominate the reduction in P_w up to rather high frequencies.

As an alternative to profiting from reduced losses, it should be possible to reduce the MFT in size and, consequently, cost. To this end, the core and conductor cross-sections are reduced, increasing the losses, either just a bit, or until they are back to those at f_sw^*. In view of this option, it is interesting to discuss what happens to the losses if the core shrinks. For this discussion, it is assumed that f_sw stays constant, and that also L_m and L_σ have fixed values as imposed by the TRS. The core volume can shrink by a

reduction of either A_c or ℓ_c, including a combination of the two. First, the effect of a reduction in A_c is analyzed. Under the assumption of a preserved inductance ratio, one finds from (6) that

$$\ell_\mathrm{g} \propto A_\mathrm{c}^{1/2}. \tag{15}$$

This implies a drop in ℓ_g. Keeping L_m constant means, according to (4), that

$$N_\mathrm{t} \propto \frac{\ell_\mathrm{g}^{1/2}}{A_\mathrm{c}^{1/2}} \propto A_\mathrm{c}^{-1/4}, \tag{16}$$

resulting in an increase in N_t. Together with (11), this means that the winding losses remain constant:

$$P_\mathrm{w} \propto N_\mathrm{t}^2 A_\mathrm{c}^{1/2} = \mathrm{const.} \tag{17}$$

To determine the scaling of the core losses, it is noted that $\ell_\mathrm{c} \propto \Delta z_\mathrm{c} + \Delta x_\mathrm{c}$. If it is assumed that the drivers of Δz_c and Δx_c are Δz_w and Δr_i, respectively, then

$$\ell_\mathrm{c} \propto 1 + \frac{\Delta r_\mathrm{i}}{\Delta z_\mathrm{w}}. \tag{18}$$

With the core volume $V_\mathrm{c} \propto A_\mathrm{c}\ell_\mathrm{c}$, and based on (5), one obtains

$$P_\mathrm{c} \propto V_\mathrm{c}\hat{B}^\beta \propto A_\mathrm{c}\left(1 + \frac{\Delta r_\mathrm{i}}{\Delta z_\mathrm{w}}\right)\left(\frac{N_\mathrm{t}\hat{I}_\mathrm{m}}{\ell_\mathrm{g}}\right)^2, \tag{19}$$

and, using (15) and (16),

$$P_\mathrm{c} \propto A_\mathrm{c}^{-1/2}. \tag{20}$$

The effect of a reduction in ℓ_c on the losses is analyzed assuming that this reduction is driven by a decrease in Δz_w. It is then noted from (6), that

$$\ell_\mathrm{g} \propto \Delta z_\mathrm{w}, \tag{21}$$

implying a reduction in air-gap width. From (3),

$$N_\mathrm{t} \propto \Delta z_\mathrm{w}^{1/2}, \tag{22}$$

one notes that the number of turns decreases. Using again (11), inserting (22), and keeping A_c constant shows that the winding losses are again constant:

$$P_\mathrm{w} \propto \frac{N_\mathrm{t}^2}{\Delta z_\mathrm{w}} = \mathrm{const.} \tag{23}$$

For the core losses, one can start from (19), fix A_c, and use (22) and (23):

$$P_\mathrm{c} \propto \left(1 + \frac{\Delta r_\mathrm{i}}{\Delta z_\mathrm{w}}\right)\left(\frac{N_\mathrm{t}\hat{I}_\mathrm{m}}{\ell_\mathrm{g}}\right)^2 \propto \left(1 + \frac{\Delta r_\mathrm{i}}{\Delta z_\mathrm{w}}\right)\frac{1}{\Delta z_\mathrm{w}}. \tag{24}$$

Scaling laws (20) and (24) demonstrate that no matter by which mechanism the core shrinks, the size reduction is accompanied by an increase in core losses, while the winding losses remain constant. Importantly, one can conclude that *if* the core is thermally limited, further size reduction will not be possible. The admissible temperatures would not only be exceeded because of the rise in P_c, but also because of the reduction in core surface and, hence, cooling surface.

Results from MFT optimization tool

Cases considered

To test the scaling laws that were developed under simplifying assumptions, parameter studies were made using designs obtained with the MFT optimization tool. Four cases were studied, which shared the TRS described in Tab. 1. They are typical for MFTs used in the cells of SSTs of ISOP topology, rated for a power in the MW range. Nanocrystalline core material (Vitroperm 500) and copper litz wire was used in accordance with the assumptions in the scaling laws. The MFT has an O-core as depicted in Fig. 1. The weighting factors w_c, w_m, w_V, and w_λ in Eq. (2) were set to 0.8, 0, 0.2, and 0, respectively. This puts a strong emphasis on cost, while also considering the volume a little to avoid weird designs that strongly grow in volume for a marginal cost benefit. No weight was attributed to λ, since the

efficiency is constrained directly, as described below. The frequencies studied are in the range of 1 to 15 kHz. The ratio L_m/L_σ was initially assumed to be constant to preserve the ratio between magnetizing and load current. This constraint is not a strict necessity and will be relaxed below.

Property	**Value**
real power	500 kW
cell voltage on HV side	750 V
HV-to-LV turns ratio	2
$2\pi f_\mathrm{sw} L_\mathrm{m}$	39.8 Ω (case 1 to 3)
L_m/L_σ	80 (case 1 to 3)
insulation	dry-cast
DC insulation voltage	25 kV
equivalent "highest voltage for equipment" U_m [16]	17.5 kV rms
1 min. applied AC test voltage [16]	38 kV rms
lightning-impulse test voltage [16]	95 kV
cooling	air forced
ambient temperature	35 °C

Tab. 1: Common MFT TRS of the cases studied with the MFT optimization tool.

Case 1 – constrained efficiency

In a first case, the efficiency was constrained by limiting the loss ratio to $\lambda_\mathrm{lim} = 0.6$ %. In Fig. 2, the MFT performance metrics V_box, C, m, and u are shown as a function of f_sw. It can be seen that in the range of 1 to about 7 kHz, the MFT benefits from the increase in frequency, with all the metrics decreasing. This corresponds to the expectations based on the developed scaling laws. However, the decrease levels off at $f_\mathrm{sw,sat} \cong 7$ kHz, and no further improvement can be observed when continuing to increase f_sw. It is concluded that $f_\mathrm{sw,sat}$ is a "scaling saturation frequency", at which the scaling laws obtained under the simplifying assumptions made cease to apply.

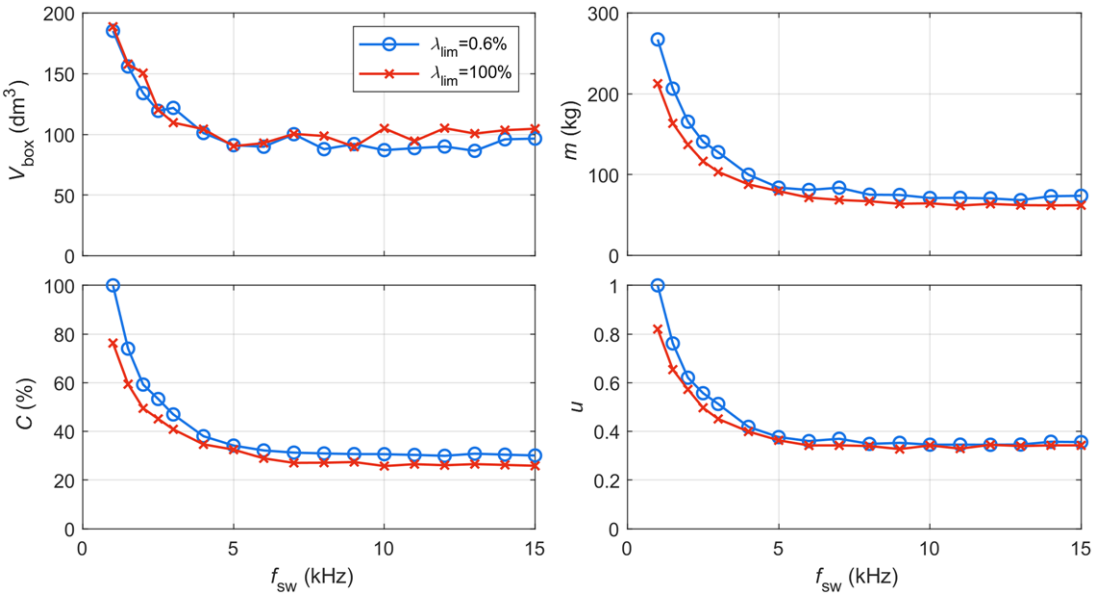

Fig. 2: Cases 1 and 2, MFT performance metrics.

To gain insight into this behavior, it is necessary to look at further MFT properties as a function of frequency. At this point, it is noted that the curves over f_sw are often not smooth, but exhibit jumps, or kinks. This has to do with the primary variables and properties of the MFT that are of integer type, such as N_t, but also d_s or the depth of nanocrystalline cores (that equals the ribbon width), because suppliers

standardize their products to discrete sizes. When, at some transition frequency, the optimum jumps from one discrete value of a property to the next, a corresponding jump in all properties results.

In Fig. 3, winding properties are summarized. Above $f_{\mathrm{sw,sat}}$, there is only a weak trend of N_t to decrease with f_sw. In contrast, below $f_{\mathrm{sw,sat}}$, the behavior resembles that of scaling law (7) derived under the assumption of a fixed MFT geometry. The DC resistance of the HV winding shows a gradual decrease with f_sw. The decrease of the AC resistance is a little weaker in comparison as a result of an increase in F_R. The loss data are shown in Fig. 4. λ equals λ_lim over the whole frequency range, indicating an active constraint. At low f_sw, about 90 % of the losses are created in the windings, and only 10 % in the core.

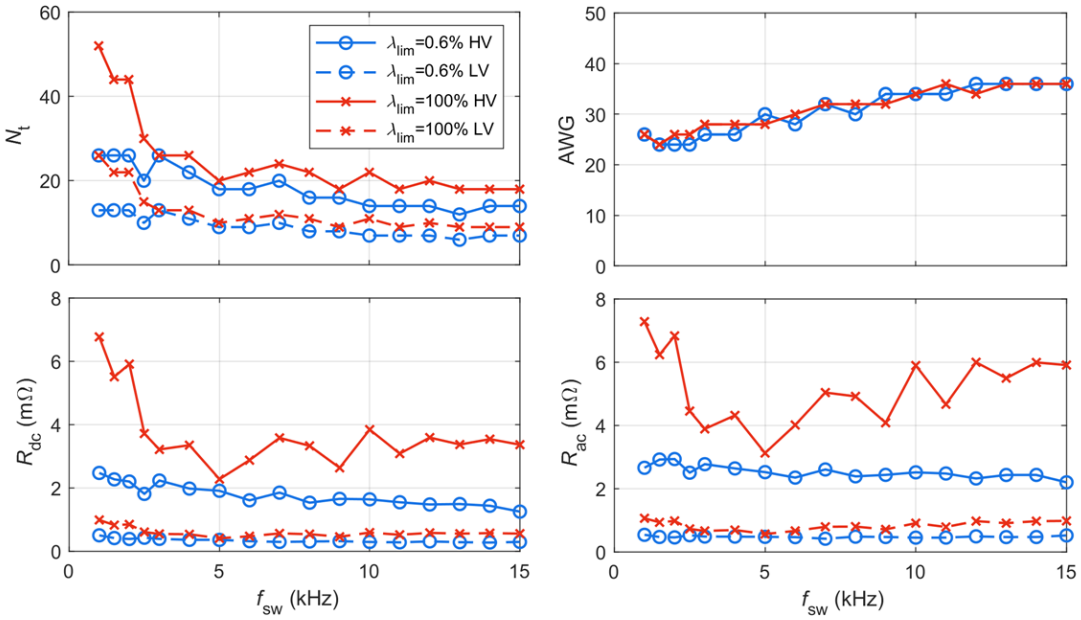

Fig. 3: Cases 1 and 2, winding properties.

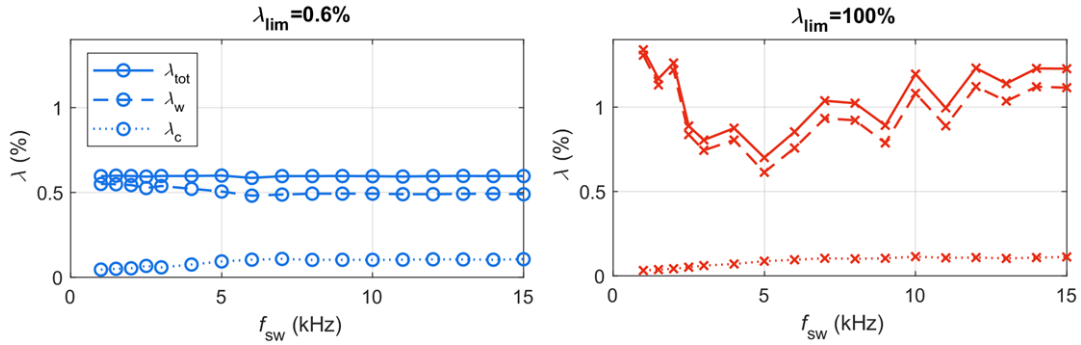

Fig. 4: Cases 1 (left) and 2 (right), loss ratio.

To understand why no benefit can be obtained by increasing f_sw beyond $f_{\mathrm{sw,sat}}$, it is instructive to look at the constraint functions that are plotted in Fig. 5. Up to about $f_{\mathrm{sw,sat}}$, the core is saturated, as indicated by the corresponding active constraint. From $f_{\mathrm{sw,sat}}$ on, the core is not saturated any more, but thermally limited. Throughout the entire frequency range studied, the constraint on λ is active, while the windings are generally not thermally limited. Referring to the scaling laws derived, the behavior below $f_{\mathrm{sw,sat}}$ can be thought of as the result of two steps: (i) increase of f_sw for fixed size, reducing the losses; and (ii) using the created loss margin to shrink the MFT according to scaling laws (17), (20), (23), and (24). These steps are useful for the understanding, while the *MFT optimization tool* finds the optimum directly by sweeping x. Importantly, below $f_{\mathrm{sw,sat}}$, the other active constraint, the one on core saturation, scales favorably with frequency, allowing the core to shrink on increasing f_sw. The core-temperature constraint, active above $f_{\mathrm{sw,sat}}$ does not scale favorably with frequency, preventing further size reduction. The behavior is confirmed in Fig. 6, where the core cost – a direct indicator of the core volume – is shown. Another important observation in Fig. 6 is that the cost of the core is at most of the

frequencies at least twice that of the windings (LV and HV winding together), and thus dominating the cost of the MFT. This shows the key role of the core in any approach to reduce MFT cost. Another constraint, which is plotted in Fig. 5, is that of the minimum air gap needed for robustness and fine-tuning of L_m. As can be seen, the constraint is always far from active, confirming that the assumptions made in the derivation of scaling law (4) are valid.

A general remark is added regarding the interpretation of the constraint functions. It is important to remember the discrete nature of the physical model of the MFT, as discussed above. Therefore, it may happened that a constraint function cannot reach exactly zero, and a negative value close to zero indicates an active constraint. The next integer value of a design variable would lead to a positive constraint-function value and a violation of the constraint.

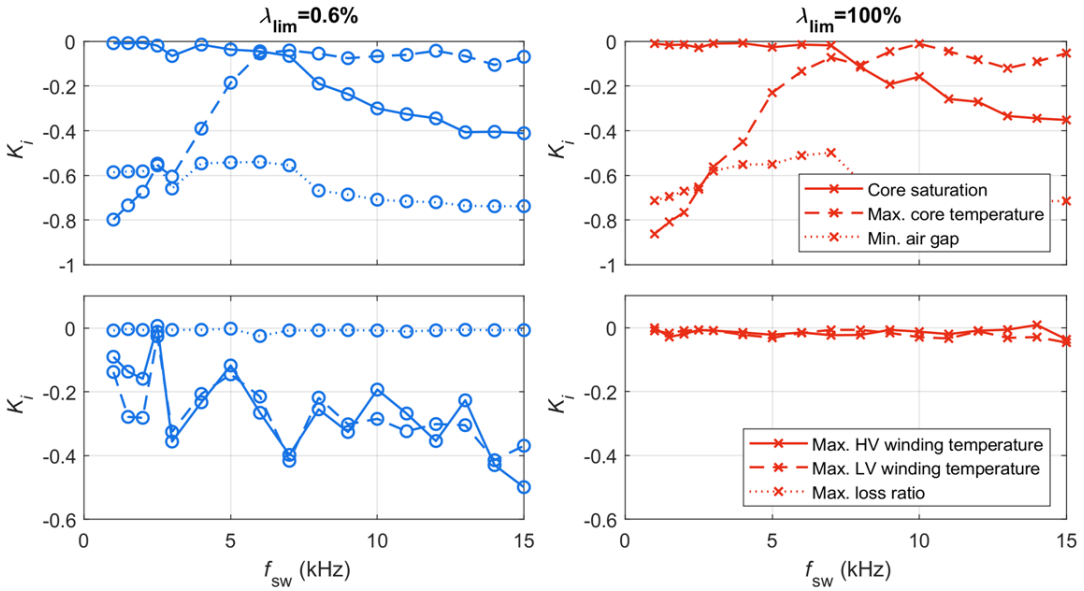

Fig. 5: Cases 1 (left) and 2 (right), constraint functions.

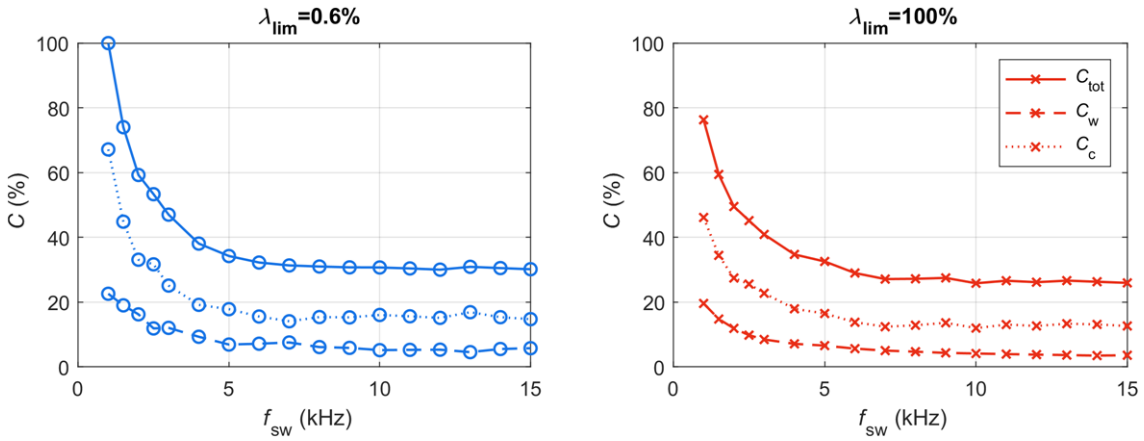

Fig. 6: Cases 1 (left) and 2 (right), MFT costs and mass.

Case 2 – unconstrained efficiency

In case 2, the efficiency constraint was relaxed to investigate its influence on the MFT performance metrics. In Fig. 2 it can be seen that, while the size increases a little, there is a slight decrease in mass and cost, resulting also in a minor decrease in u. Overall, there is a parallel shift of curves rather than a more pronounced scaling with f_sw. In particular, $f_\mathrm{sw,sat}$ remains at about 7 kHz.

As can be seen in Fig. 3, compared to case 1 there is a noticeable increase in N_t at low frequencies, which enables the core to shrink and leads to a significant increase in losses. It is concluded that the loss-ratio constraint has been the limiting factor preventing this in case 1. Above $f_\mathrm{sw,sat}$, N_t also increases compared to case 1, but less than at low frequencies. The result is the same, i.e., a reduction

in core size (as confirmed in Fig. 6) at the expense of higher losses. The new limiting constraint is the winding temperature. From $f_{\mathrm{sw,sat}}$ on, the core temperature is also at or near the limit, as the corresponding constraint function is close to zero. Hence, it can be concluded that in case 2 the MFT is entirely thermally limited. Further size and cost reduction of the MFT can only be enabled through more aggressive cooling.

Case 3 – unconstrained efficiency, better core cooling

Regarding the thermal limitation found in case 2, the key role of the core is noted again, and its dominant contribution to cost. Therefore, in a third case, the influence of cooling efficiency was studied. Cases 1 and 2 had a heat-transfer coefficient (HTC) between core surface and air of 36 $\mathrm{W/(m^2K)}$, corresponding to realistic forced air cooling with an air speed of several $\mathrm{m/s}$. More aggressive cooling with the HTC doubled to 72 $\mathrm{W/(m^2K)}$ shifts $f_{\mathrm{sw,sat}}$ up from 7 to about 16 kHz. The winding losses, and thereby the total losses, are slightly reduced (with λ dropping by up to 0.2 %) thanks to smaller core cross-section. This behavior is remarkable, since often, better cooling is only an enabler of *higher* losses.

Case 4 – variation of constraints on inductances

A fourth case was included to study the influence of the inductance constraints, again for unconstrained loss ratio. The results are summarized in Fig. 7. With L_{m} still constrained, the blue and green curves show the effect of a deviation of L_{m}/L_σ from the baseline value of 80. The grey curves are for relaxed L_{m}/L_σ constraint, and the black ones for additionally relaxed L_{m}. It is observed that $L_{\mathrm{m}}/L_\sigma = 80$ is close to the natural value of L_{m}/L_σ, while the natural value of L_{m} is higher than the originally prescribed value of 39.8 $\Omega/(2\pi f_{\mathrm{sw}})$. Interestingly, once the constraint on L_{m}/L_σ has been relaxed, the additional relaxation of L_{m} does not lead to any change. For L_{m}/L_σ below its natural value, the cost function increases slightly below $f_{\mathrm{sw,sat}}$, while for L_{m}/L_σ above its natural value, there is a more pronounced increase of the cost function above $f_{\mathrm{sw,sat}}$. Overall, it can be concluded that there is significant flexibility in the choice of the inductances without a major drawback in terms of cost function, while the value of $f_{\mathrm{sw,sat}}$ remains largely unchanged.

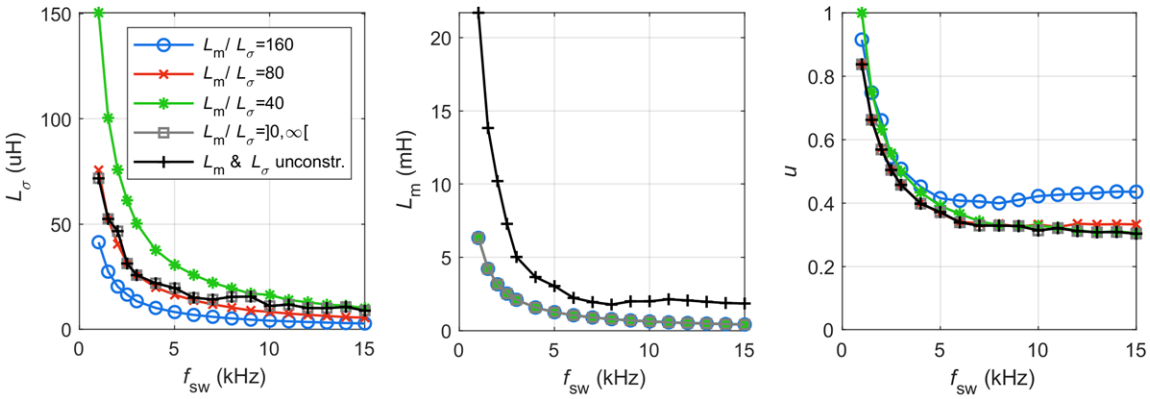

Fig. 7: Case 4, inductances and cost function.

Conclusion

Economic MFTs are a key enabler for economic SSTs and MVDC solutions. An understanding of the influences on the MFT cost structure, and of the limitations to the reduction of size, mass, and cost, is therefore key. Simplified scaling laws suggest a potential of an increase in switching frequency to improve the MFT performance metrics. They suggest that for fixed MFT geometry, an increase in frequency can lead to lower losses under constrained inductances. Alternatively, the size can be reduced while reducing the losses less or keeping them constant. The scaling laws also show that a core-size reduction at a given frequency must always be accompanied by increasing core losses.

In practical MFT design, size reduction is only observed up to a certain "scaling saturation" frequency. The analysis of the constraint functions used in the MFT optimization provides insight into this behavior. In case of the loss ratio constrained to ≤ 0.6 %, this constraint limits the designs at all frequencies. In particular, core-size reduction is not possible, even though the core's contribution to the total losses is

modest. Relaxing the loss constraint leads to moderately smaller designs, while increasing the losses significantly, but does not shift the scaling saturation frequency. The designs are thermally limited in this case. Improving the core cooling shows the key role of the core in MFT design, in particular in terms of cost contribution. An upward shift in the scaling saturation frequency can be achieved, resulting in cost savings without a penalty of increased losses. The results hence clearly indicate that too weak core cooling should be avoided in MFTs using nanocrystalline cores.

Overall, the results suggest that, for the considered MFT technology, there is little motivation to increase the switching frequency of the converter beyond about 7 kHz, which is the scaling saturation limit. Higher frequencies, however, may still be interesting from the point of view of acoustic noise. Switching at 10 kHz, for example, allows to safely move the noise out of the audible range, in particular with the core's magnetostriction emitting noise at twice the switching frequency.

References

[1] World's first 5 MW DC converter, https://impulse.schaffner.com/de/power-magnetics-5-mw-gleichstromwandler, 29 October 2021.

[2] C. Zhao, D. Dujic, A. Mester, J. K. Steinke, M. Weiss, S. Lewdeni-Schmid, T. Chaudhuri, and P. Stefanutti, "Power electronic traction transformer – medium voltage prototype", IEEE Trans. on Industrial Electronics, vol. 61, no. 7, pp. 3257–3268, July 2014.

[3] D. Dujic, "Electric vehicles charging – an ultrafast overview", keynote at PCIM Asia, Int. Exhibition and Conf. for Power Electronics, Intelligent Motion, Renewable Energy and Energy Management, Shanghai, China, 26–28 June 2019.

[4] X. Wang, "Optimal DC power distribution system design for data center with efficiency improvement", PhD thesis, University of Wisconsin-Milwaukee, August 2014.

[5] L. Wang, F. Zhang, J. A. Aroca, A. V. Vasilakos, K. Zheng, C. Hou, D. Li, and Z. Liu, "GreenDCN: a general framework for achieving energy efficiency in data center networks", IEEE Journal on Selected Areas in Communications, vol. 32, no. 1, pp. 4-15, January 2014.

[6] M. K. Das, C. Capell, D. E. Grider, S. Leslie, J. Ostop, R. Raju, M. Schutten, J. Nasadoski, and A. Hefner, "10 kV, 120 A SiC half H-bridge power MOSFET modules suitable for high frequency, medium voltage applications", IEEE Energy Conversion Congress and Exposition, pp. 2689-2692, September 2011.

[7] D. Wang, J. Tian, C. Mao, J. Lu, Y. Duan, J. Qiu, and H. Cai, "A 10-kV/400-V 500-kVA electronic power transformer", IEEE Trans. on Industrial Electronics, vol. 63, no. 11, pp. 6653–6663, November 2016.

[8] J. Yu, K. Smith, M. Urizarbarrena, N. MacLeod, R. Bryans, and A. Moon, "Initial designs for the ANGLE DC project; converting existing AC cable and overhead line into DC operation", 13th IET Int. Conf. on AC and DC Power Transmission (ACDC), pp. 1-6, 2017.

[9] M. Mogorovic, "Modeling and design optimization of medium frequency transformers for medium-voltage high-power converters," PhD thesis, EPFL Lausanne, Switzerland, 2019.

[10] U. Drofenik, "A 150 kW medium frequency transformer optimized for maximum power density", 7th Int. Conf. on Integrated Power Electronics Systems (CIPS), Nuremberg, Germany, 6–8 March 2012.

[11] M. Mogorovic and D. Dujic, "Sensitivity analysis of medium frequency transformer design", Int. Power Electronics Conference (IPEC-Niigata – ECCE Asia), pp. 2170-2175, 2018.

[12] M. Mogorovic and D. Dujic, "Sensitivity analysis of medium-frequency transformer designs for solid-state transformers", IEEE Trans. on Power Electronics, vol. 34, no. 9, pp. 8356-8367, September 2019.

[13] N. Mohan, T. M. Undeland, and W. P. Robbins, "Power electronics: converters, applications, and design", 3rd ed., John Wiley & Sons, 2002.

[14] T. Gradinger and M. Mogorovic, "Foil-winding design for medium-frequency medium-voltage transformers", 23rd European Conf. on Power Electronics and Applications (EPE ECCE Europe), online, 6–10 September 2021.

[15] A. Van den Bossche and V. C. Valchev, "Inductors and transformers for power electronics", Taylor & Francis, March 2005.

[16] IEC 60076-3, 2nd ed., "Power transformers – Part 3: Insulation levels, dielectric tests and external clearances in air", March 2000.

[17] M. Mogorovic and D. Dujic, "Analysis of the effectiveness of the series inductor integration into the MFT for SST Applications", PCIM Europe digital days, Intern. Exhibition and Conf. for Power Electronics, Intelligent Motion, Renewable Energy and Energy Management, pp. 1-7, 2020.